PAPER

Check for updates

Tuning the optical properties in CsPbBr₃ quantum dot-doped glass by modulation of its network topology

Zhousu Xu, [iD] †[a] Tao Chen,†[a] Duoduo Zhang,[b] Guojun Zheng,[d] Zhuo Wang,[d] Zhijun Ma, [iD] [f] Jinhua Yan,[a] Xianwei Wang, [iD] [a] Xiaofeng Liu [iD] *[bc] and Jianrong Qiu*[de]

All inorganic metal halide perovskite quantum dots (QDs) exhibit excellent optical properties promising for diverse applications, while their inherent frangibility remains an enormous challenge for both scientific research and practical applications. Recently emerged oxide glasses doped with such QDs exhibit high stability against degradation and are thus highly promising for photonic applications. Here, we demonstrate the tuning of the linear and nonlinear optical properties of perovskite QD-doped glass through modulation of its network topology. By introducing a metal fluoride network modifier, we show that the precipitation of the QDs can be promoted as a result of the enhanced ion mobility during heat treatment. The QD-doped glasses show strong one-photon and two-photon upconversion photoluminescence (PL). Also, the PL intensity can be enhanced by up to 800% for the sample with an optimal local structure. In addition, the control of QD precipitation by modulating the glass network topology could allow for the observation of a cross-over from saturable absorption to reverse saturable absorption. The methodology for tuning the optical properties of QD-in-glass composites studied here might be applied for the design of photonic glasses for relevant applications.

1. Introduction

Owing to the excellent tunable photoluminescence (PL) emission covering the entire visible spectral region (400–700 nm) with high photoluminescence quantum yield (PLQY), all-inorganic cesium lead halide (CsPbX₃, X = Cl, Br, and I) perovskite quantum dots (QDs) have attracted tremendous attention,[1–3] as these unique features could endow CsPbX₃ QDs with great potential for applications in various fields, such as solar cells, displays, lasers, and light-emitting diodes (LEDs).[4–8] The synthesis of these QDs has been realized by both chemical and physical

processes, such as the spin-coating method,[9–11] sol–gel method,[12–14] co-deposition in solution method,[15,16] and molecular beam epitaxy method.[17–19] Recently, all-inorganic perovskite QDs have also been precipitated in different oxide glasses by a conventional melt–quenching–annealing method.[20–34] The oxide glass matrix offers strong protection needed by the incorporated perovskite QDs against thermal, chemical, and optical degradation. In addition, this method provides a convenient way for precipitating all-inorganic perovskite QDs in glasses with a controllable concentration and size, which allows for tuning their optical performances.

The use of a glass matrix for QDs offers additional benefits as the composition and properties of the glass can be carefully tuned to control the formation and the optical properties of the precipitated QDs. Similar to the wet-chemistry route, the control of the growth conditions such as the temperature and duration could allow for the modulation of the QD size and concentration, which strongly affects the optical properties of QDs. On the other hand, the glass matrix itself could be designed to control the growth of QDs by modulating its network topology. For instance, the introduction of alkali earth metal fluoride could result in the modification of the network structure as F⁻ ions can replace the bridge oxygen position, making the bridge oxygen into non-bridge oxygen and breaking

[a] *Institute of Intelligent Optoelectronic Technology, Zhejiang University of Technology, Hangzhou, 310014, China*

[b] *School of Materials Science and Engineering, Zhejiang University, Hangzhou, 310027, China. E-mail: xfliu@zju.edu.cn*

[c] *Wuhan National Laboratory for Optoelectronics, Wuhan, 430074, China*

[d] *State Key Laboratory of Modern Optical Instrumentation, College of Optical Science and Engineering, Zhejiang University, Hangzhou, 310027, China. E-mail: qjr@zju.edu.cn*

[e] *CAS Center for Excellence in Ultra-intense Laser Science, Jiading, Shanghai 201800, China*

[f] *State Key Laboratory of Luminescent Materials and Devices, and Institute of Optical Communication Materials, South China University of Technology, Guangzhou 510641, China*

† These authors contributed equally to this work.

This journal is © The Royal Society of Chemistry 2021

J. Mater. Chem. C, 2021, **9**, 6863–6872 | **6863**

the tight glass network, which is beneficial for the movement of the ions and the nucleation and growth of crystals inside the glass.[35–38] Moreover, the low vibration energy of the metal fluorine bond compared to that of the metal–oxygen bond could result in the reduction of phonon energy of the glass host, so that the non-radiative transition probability is reduced, and the PL intensity and PLQY are increased.[39–41]

In this investigation, we study the tuning of the optical performance of $CsPbBr_3$ perovskite QDs precipitated in a borosilicate glass by modulating the network topology based on the conventional melt–quenching–annealing technique. CaF_2 is employed as the network modifier which strongly modifies the connectivity of oxygen atoms and the local structure of the examined glass. The results indicate that the formation of QDs and their linear and nonlinear optical properties are strongly dependent on the glass structure. The methodology demonstrated in the present work could be further exploited for the development of glass-based photonic materials.

2. Experiment

2.1. Synthesis of $CsPbBr_3$ QD-doped glass

$CsPbBr_3$ QD-doped glasses were prepared using the conventional melting–quenching method. The molar composition of $CsPbBr_3$ QD-doped glass is $38SiO_2$–$34B_2O_3$–$11ZnO$–$6Cs_2CO_3$–$2PbO$–$9NaBr$–$xCaF_2$ ($x = 0$, 0.5, 1, 2, 3, 4, and 5), and raw powder materials were mixed thoroughly and melted at 1100 °C for 30 min to form precursor glass samples. Then, the precursor glasses were heat-treated at 440–480 °C for 10 h to precipitate $CsPbBr_3$ perovskite QDs. Eventually, all the glass samples were cut and polished for optical measurements. The glass samples were denoted as CPBx–y–z, where x is the molar fraction of the added CaF_2, and y and z are the heat treatment temperature and duration, respectively.

2.2. Characterization

X-ray diffraction (XRD) patterns were recorded using an X'Pert PRO powder diffractometer with Cu Kα radiation (PANalytical, Holland). Microstructure characterization was performed with a Tecnai G2 F30 S-Twin high-resolution transmission electron microscope (HRTEM) (Philips-FEI Instruments, Holland). Fourier transform infrared (FTIR) spectra were recorded by using a Nicolet 6700 spectrometer (Thermo Fisher Scientific Inc., Waltham, MA, USA). Raman spectra were recorded for the glass samples by using an InVia Reflex Raman spectrometer (Renishaw, UK) using a 532 nm diode laser as the excitation source. Differential scanning calorimetry (DSC) curves were recorded by using SDT Q600 simultaneous thermal analyzers (TA Instruments, USA). Absorption spectra were recorded with a UV-3600 UV-VIS-NIR spectrophotometer (Shimadzu Instruments, Japan). PL spectra were recorded by using a FLS980 fluorescence spectrometer (Edinburgh Instruments, UK). The PL quantum yield (QY) was measured by using an absolute photoluminescence quantum yield measurement system (Quantaurus-QY Plus C13534-35, Japan). The refractive index of the sample was measured by using a Model 2010/M prism coupler (Metricon Instruments).

2.3. Z-scan measurement

An open aperture Z-scan system was employed to investigate the NLO properties of the $CsPbBr_3$ QD-doped glass, using a femtosecond laser (central wavelength: 1030 nm, pulse duration: 226 fs, and repetition rate: 10 kHz) as the excitation source.

3. Results and discussion

We use a borosilicate glass as the matrix as it can be melted at a temperature of 1100 °C, at which the metal halide reactive species suffer moderate evaporation loss. CaF_2, a stable fluoride with a melting temperature (1423 °C) close to the glass melt, was introduced to this glass as an additional network modifier that breaks the oxygen bridges and facilitates the mobility of ions needed for the formation of the QDs.

As can be seen from Fig. 1(a), the color of the samples changes from light green to yellow, depending on the CaF_2 concentration and heat-treatment temperature. Under irradiation from a 365 nm ultraviolet (UV) lamp, strong PL is observed and the PL intensity is high for samples with a green color (Fig. 1(b)). Fig. 1(c) shows the X-ray diffraction (XRD) patterns of the glass samples CPBx-470-10 ($x = 0$, 1, 3, and 5). Several diffraction peaks are observed at angles (2θ) of approximately 21.4°, 30.4°, 37.5°, 43.5°, and 58.9° for the samples CPB1-470-10, CPB3-470-10, and CPB5-470-10, corresponding to the (110), (200), (211), (220) and (310) planes of $CsPbBr_3$ QDs (PDF#54-0752), respectively, which indicates the successful precipitation of $CsPbBr_3$ perovskite QDs in the glasses. Compared with the sample CPB0-470-10, the samples CPB1-470-10 and CPB3-10-2.5 show strong diffraction peaks, as shown in Fig. 1(c) and (e). The XRD patterns show that the addition of CaF_2 is favourable for the crystallization of $CsPbBr_3$ QDs in the glass. Sample CPB5-470-10 has an additional diffraction peak at 46.9°, corresponding to the (200) plane of the CaF_2 crystal (PDF#35-0816), which indicates that the CaF_2 crystal was also precipitated in the glass matrix. The XRD patterns of the glass samples obtained at different heat-treatment temperatures were also recorded, as shown in Fig. 1(d). The result shows that the intensity of the diffraction peak of glass samples CPB3-y-10 increases with the increase of heat-treatment temperature from 440 °C to 480 °C, which implies the enhancement of crystallinity and concentration of $CsPbBr_3$ QDs in the glasses. To understand the network structure of the glass samples, Fourier transform infrared (FTIR) spectra and Raman spectra were recorded. To avoid self-fluorescence of the $CsPbBr_3$ QDs in the Raman spectrum measurement, the glass samples without $CsPbBr_3$ QDs were prepared by removal of PbO from the glass compositions. Four main absorption bands can be observed in the FTIR spectra, as shown in Fig. 1(f). The absorption bands of the $[BO_3]$ triangle (located at 695–705 cm^{-1} and 1380–1400 cm^{-1}), $[BO_4]$ tetrahedron (1020–1060 cm^{-1}), and $[SiO_4]$ tetrahedron (695–705 cm^{-1} and 1020–1060 cm^{-1}) can be clearly observed.[42] These groups are also captured in the Raman spectra, while the intensities are

6864 | J. Mater. Chem. C, 2021, 9, 6863–6872

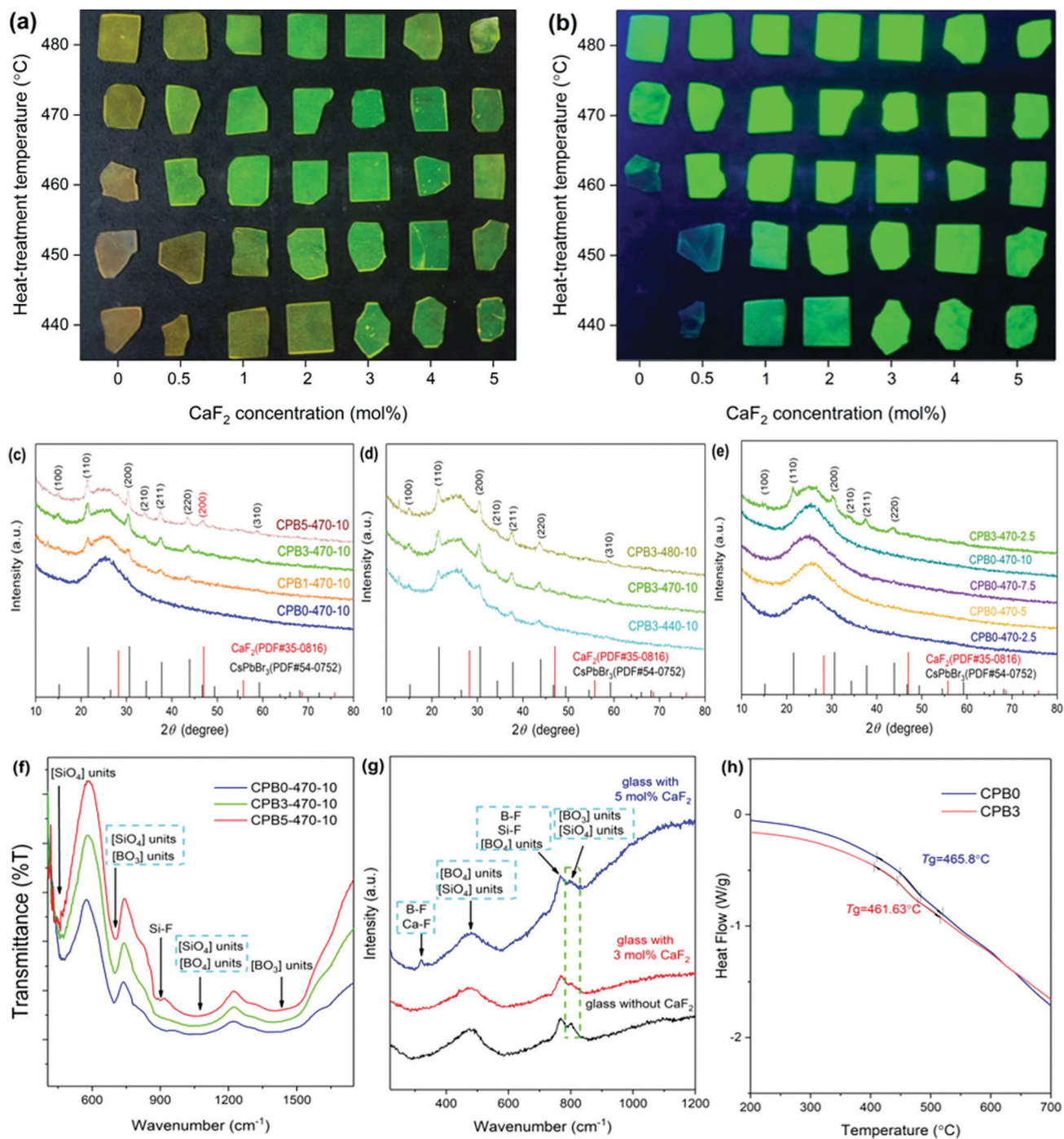This journal is © The Royal Society of Chemistry 2021

Fig. 1 (a and b) Photographs of glass samples under illumination of (a) daylight and (b) UV lamp. (c and d) XRD patterns of glass samples (c) with different CaF$_2$ concentrations, (d) with different heat-treatment temperatures, and (e) with different heat-treatment durations at 470 °C for samples of CPB0-470-z and CPB3-470-z (z is the heat treatment duration in hours). (f) FT-IR spectra of glass samples of CPB0-470-10, CPB3-470-10, and CPB5-470-10. (g) Raman spectra of borosilicate glasses without and with CaF$_2$. (h) DSC curves of glass samples of CPB0 and CPB3.

different,[43,44] as shown in Fig. 1(g). The FTIR and Raman spectra results indicate that the borosilicate glass network mainly consists of a [BO$_3$] triangle, [BO$_4$] tetrahedron and [SiO$_4$] tetrahedron through the interconnection of apical oxygen atoms. With the addition of CaF$_2$ into the glass, an extra absorption band appears at approximately 900 cm^{-1} in the FT-IR spectra, which can be ascribed to the Si–F bond.[45,46] Moreover, the formation of B–F and

Ca–F bonds is also evidenced from the Raman spectra.[47,48] With the increase in the CaF$_2$ concentration, the Raman peak intensity at around 800 cm^{-1} due to bridged oxygen decreases, while the peak at 768 cm^{-1} contributed from both bridge oxygen (B–O) and non-bridge oxygen bonds (B–F, Si–F) remains almost unchanged.[43,44,49–51] This observation implies that the added F$^-$ ions break the strong oxygen bridge (i.e., O–Si–O and O–B–O) to

This journal is © The Royal Society of Chemistry 2021

J. Mater. Chem. C, 2021, 9, 6863–6872 | **6865**

produce non-bridge oxygen bonds (Si–F, B–F) and thus change the network topology structure, which is beneficial for the movement of the ions and the nucleation and growth of the QDs inside the glass during heat treatment. This result is consistent with the change in the thermal stability of the samples. Fig. 1(h) shows the differential scanning calorimetry (DSC) curves of the glass samples with different CaF_2 concentrations before heat-treatment. The glass transition temperature (T_g) of 461.63 °C with the addition of 3 mol% CaF_2 is lower than that of the sample without CaF_2 (465.8 °C), indicating that the addition of CaF_2 can effectively reduce the T_g as a result of the change in the glass topology structure.

The precipitation of $CsPbBr_3$ QDs in the glass was further confirmed by transmission electron microscopy (TEM) observation, as shown in Fig. 2. Fig. 2(a) and (b) clearly show that a large number of nanoparticles (NPs) are dispersed in the glass. As shown in Fig. 2(c) and (d), the plane spacing values are approximately 0.261 nm and 0.291 nm, which correspond to the (210) and (200) crystal planes of $CsPbBr_3$ NCs (PDF#54-0752), respectively. Fig. 2(e) and (f) show the selected area electron diffraction (SAED) patterns of CPB0-470-10 and CPB3-470-10, respectively. The diffraction rings of CPB0-470-10 and CPB3-470-10 correspond to the (211) plane and the (200) plane of $CsPbBr_3$ nanocrystals (NCs), respectively. These results confirm that $CsPbBr_3$ QDs are precipitated in the glass matrix.

Fig. 3(a) and (b) show the absorption spectra of glass samples CPB*x*-470-10 and CPB3-*y*-10. After doping with CaF_2, the absorption edge shifts from 340 nm to 530 nm. In addition, the absorption edge shows a small red-shift with the increase in the heat-treatment temperature. According to the XRD results (Fig. 1(c) and (d)), we know that the addition of the appropriate

amount of CaF_2 and the enhancement of heat-treatment temperature could promote the crystallization of $CsPbBr_3$ QDs, which leads to the red-shift of the absorption edge. The excitation spectra of the glass samples with different CaF_2 concentrations are shown in Fig. 3(c). Broad excitation bands are observed in the visible wavelength region. With the increase of the CaF_2 concentration, the intensity of the excitation spectra first increases then decreases, implying a change in the QD size and concentration.

The emission spectra under excitation at 400 nm are shown in Fig. 3 (d)–(f), and the characteristics of the emission spectra are given in Tables 1 and 2. As the concentration of CaF_2 increases, we observe a clear red-shift in the PL peak from 516 nm to 538 nm, which is mainly attributed to the increase of the QD size due to a high growth rate in samples with higher CaF_2 content. The growth process of the $CsPbBr_3$ QDs is mainly attributed to Oswald ripening, in which the small QDs gradually attach to the large QDs, resulting in the increase of the QDs' average size.[52–54] The accelerated growth of the QDs in glass with CaF_2 can be attributed to the enhanced ion mobility due to the decreased connectivity in the glass network topology. As the heat treatment temperature increases, the PL peak wavelength red-shifts from 530 nm to 538 nm, which is also attributed to the increase of the QD size at high heat treatment temperatures. The PL intensity reaches the maximum value for the sample CPB3-470-10, which is 8 times greater than that of the glass sample without CaF_2, as shown in Table 1. Fig. 3(e) shows that the PL intensity first increases and then decreases with the increase of the CaF_2 concentration. There are two main factors for the enhancement of PL intensity after the addition of CaF_2. First, an appropriate amount of fluoride additive is favorable for
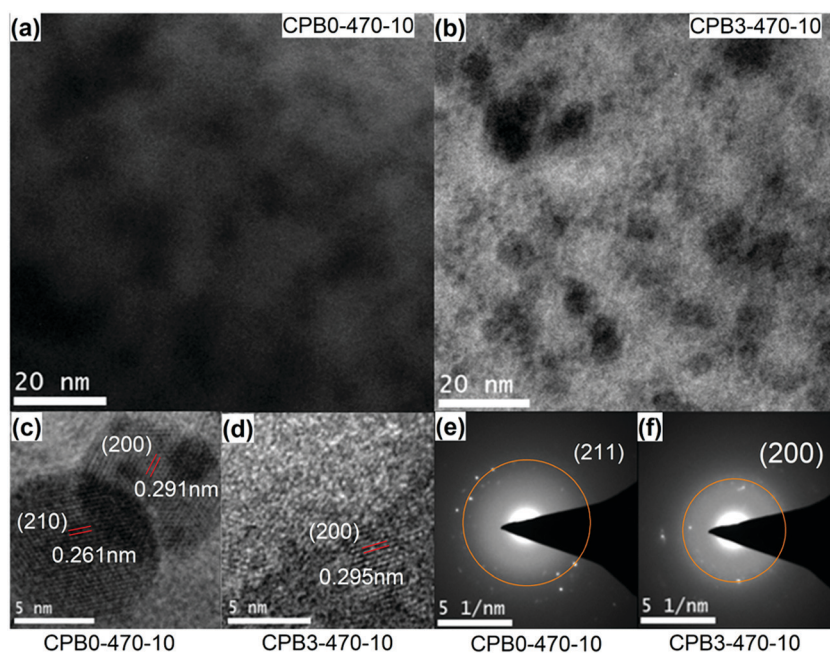

Fig. 2 (a and b) TEM images of glass samples CPB0-470-10 and CPB3-470-10. (c and d) HRTEM images of glass samples CPB0-470-10 and CPB3-470-10. (e and f) SAED images of CPB0-470-10 and CPB3-470-10.
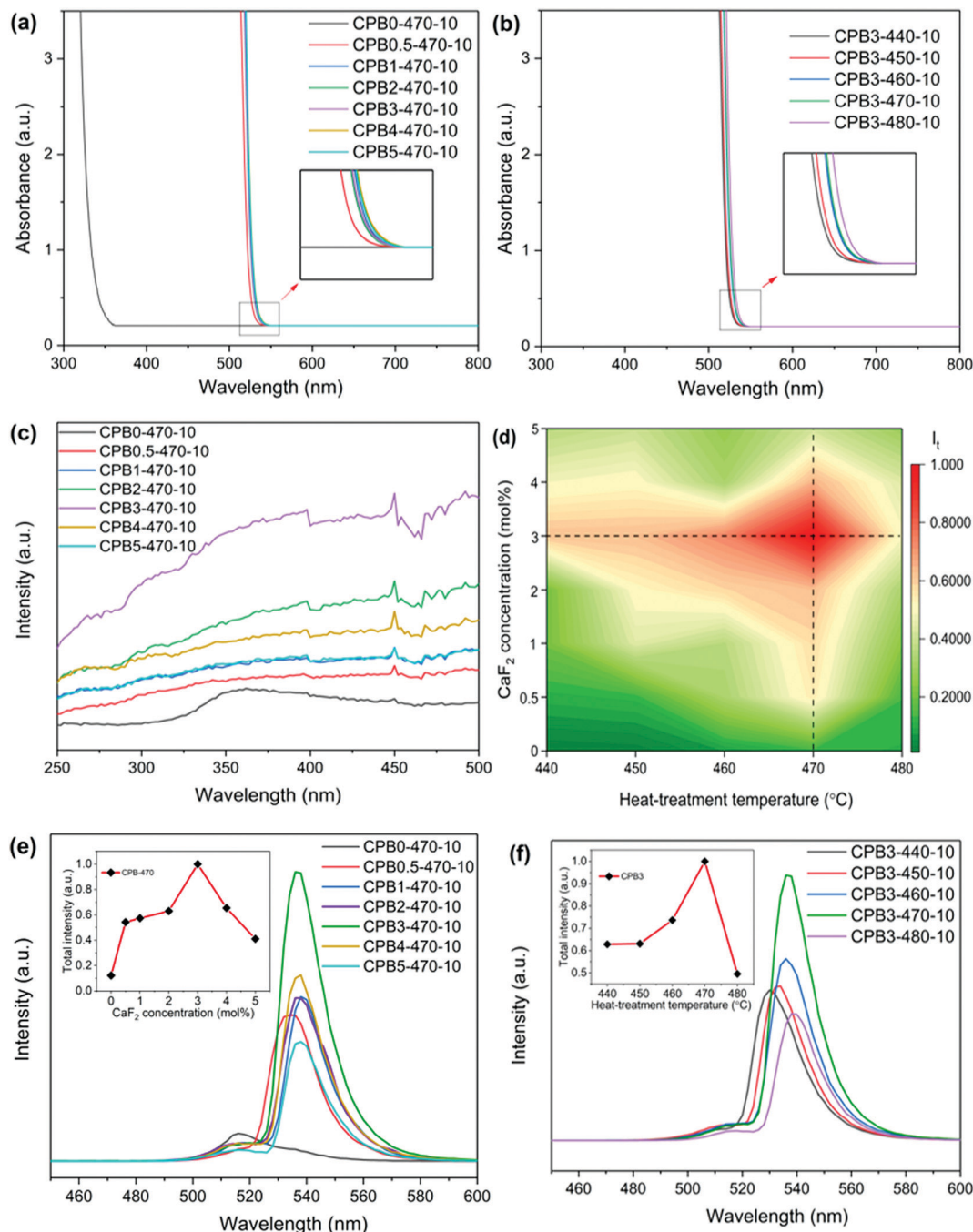
6866 | *J. Mater. Chem. C*, 2021, **9**, 6863–6872

This journal is © The Royal Society of Chemistry 2021

Fig. 3 (a and b) Absorption spectra of glass samples, (a) with different CaF$_2$ concentrations and (b) different heat-treatment temperatures. (c) Excitation spectra of glass samples with different CaF$_2$ concentrations. (d) Two-dimensional (2D) maps of integrated PL intensity as functions of CaF$_2$ concentration and heat-treatment temperature. (e and f) Emission spectra of glass samples, (e) with different CaF$_2$ concentrations and (f) different heat-treatment temperatures. (The insets show the dependence of integrated PL intensity on (e) CaF$_2$ concentration and (f) heat-treatment temperature).

the crystallization of CsPbBr$_3$ perovskite QDs in the oxide glass as the T_g is reduced due to the decrease in the network connectivity. Second, the addition of metal fluoride can effectively reduce the phonon energy of the glass and decrease the rate of nonradiative transition. Fig. 3(f) shows that the PL intensity first increases and then decreases with the increase of heat-treatment temperature. As a higher heat-treatment temperature could lead to an increase of precipitated QD concentration (also observed by

absorption), the self-absorption and the coupling among QDs could prohibit the further increase of PL intensity.

In order to further investigate the PL properties, we measured the QY of glass samples, as given in Fig. 4(a) and (b), Tables 1 and 2. It is found that the QY first increases and then decreases with the increase of heat-treatment temperature or CaF$_2$ concentration, as shown in Fig. 4(a) and (b), which is similar to the change of PL intensity. Compared with the QY of the glass

This journal is © The Royal Society of Chemistry 2021

J. Mater. Chem. C, 2021, **9**, 6863–6872 | **6867**

Table 1 Spectroscopic properties of glass samples with different CaF$_2$ concentrations

Sample	λ_p (nm)	I_t (a.u.)	QY (%)
CPB0-470-10	516	0.12	15.4
CPB0.5-470-10	534	0.54	20.1
CPB1-470-10	538	0.57	27.4
CPB2-470-10	536	0.63	36.7
CPB3-470-10	536	1	40.4
CPB4-470-10	538	0.65	30.5
CPB5-470-10	538	0.41	22.5

Note: λ_p denotes the PL peak wavelength. I_t denotes the PL total intensity, which is obtained by calculating the spectral integral area.

Table 2 Spectroscopic properties of glass samples with different heat-treatment temperatures

Sample	λ_p (nm)	I_t (a.u.)	QY (%)
CPB3-440-10	530	0.62	28.0
CPB3-450-10	534	0.63	31.4
CPB3-460-10	536	0.73	37.6
CPB3-470-10	536	1	40.4
CPB3-480-10	538	0.46	27.2

Note: λ_p denotes the PL peak wavelength. I_t denotes the PL total intensity, which is obtained by calculating the spectral integral area.

sample CPB0-470-10 without CaF$_2$, the QY of CBP3-470-10 increases by around 300% under optimized fabrication conditions. In addition, the QY values decrease with the red-shift of the excitation wavelength due to reduced absorption.

The manipulation of the network topology by introducing CaF$_2$ into the glass also enables the control of the nonlinear optical (NLO) absorption and nonlinear PL of the precipitated QDs. To examine the NLO response of the CsPbBr$_3$ perovskite QD-doped glasses, we first measured the NLO absorption using the Z-scan technique under femtosecond pulsed laser excitation at 1030 nm. The open-aperture (OA) Z-scan transmittance curves

are shown in Fig. 5. The experimental results show that the CsPbBr$_3$ QD-doped borosilicate glass exhibits a clear nonlinear absorption (NLA) response. With the increase of the CaF$_2$ concentration, the NLA response of the glass samples CPBx-470-10 changes from the saturable absorption (SA) process to the reverse saturable absorption (RSA) process, as shown in Fig. 5 (a). With the laser power increasing from 10 mW to 50 mW, the NLA response of the glass sample CPB0-470-10 also changes from the SA process to the RSA process, as shown in Fig. 5 (b). Similar laser intensity-dependent transformation from the SA to the RSA has been previously reported in other semiconductor nanomaterials or nanomaterials, such as GaAs semiconductors, WS$_2$ two-dimensional (2D) semiconductors, Cu$_{2-x}$Se NPs, Pd NPs, black phosphorus nanoplatelets and SnSe Nanosheets.[55–60] Generally, the change from the SA process to the RSA process indicates a transition from single-photon absorption (SPA) to two-photon absorption (TPA).

According to the NLO theory,[61–64] we can calculate the parameters related to NLA of glass sample CPB3-470-10 by fitting the OA Z-scan transmittance curves, including nonlinear absorption coefficient (β) and the imaginary part of the third-order NLO susceptibility (Im $\chi^{(3)}$). The refractive index of the glass sample CPB3-470-10 is 1.52. The calculated results are given in Table 3. The β and Im$\chi^{(3)}$ values of sample CBP3-470-10 decrease with the increase of laser power, as shown in Table 3, which indicates that the RSA response becomes saturated. The highest value of Im$\chi^{(3)}$ is about 8.29×10^{-13} esu, which is close to the previously reported results for colloidal CsPbBr$_3$ QDs in ref. 65 and 66.

According to the linear absorption spectra given in Fig. 3(a) and (b), the absorption edges are located at approximately 530 nm and the calculated energy of the direct bandgap is about 2.33 eV, which is much larger than the energy of the fs laser photon (1.20 eV) in our measurement. For semiconductor QD materials, when the energy of laser photons is lower than the energy of the direct bandgap, the SA nonlinear process is
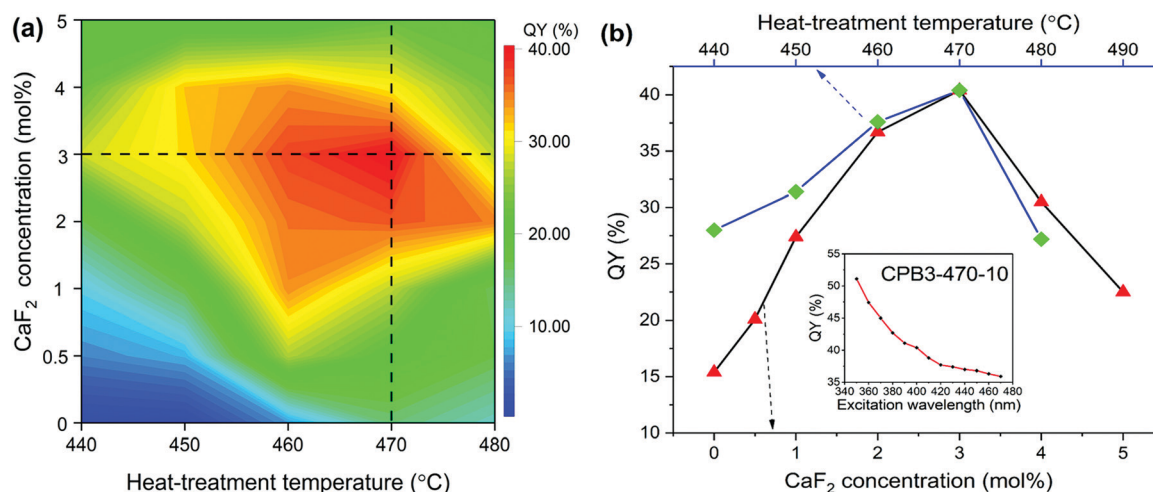

Fig. 4 (a) 2D map of QY with respect to CaF$_2$ concentration and heat-treatment temperature under 400 nm wavelength excitation. (b) The dependence of the QY on the CaF$_2$ concentration and heat-treatment temperature. (The inset shows the QY of sample CPB3-470-10 under different excitation wavelengths.)
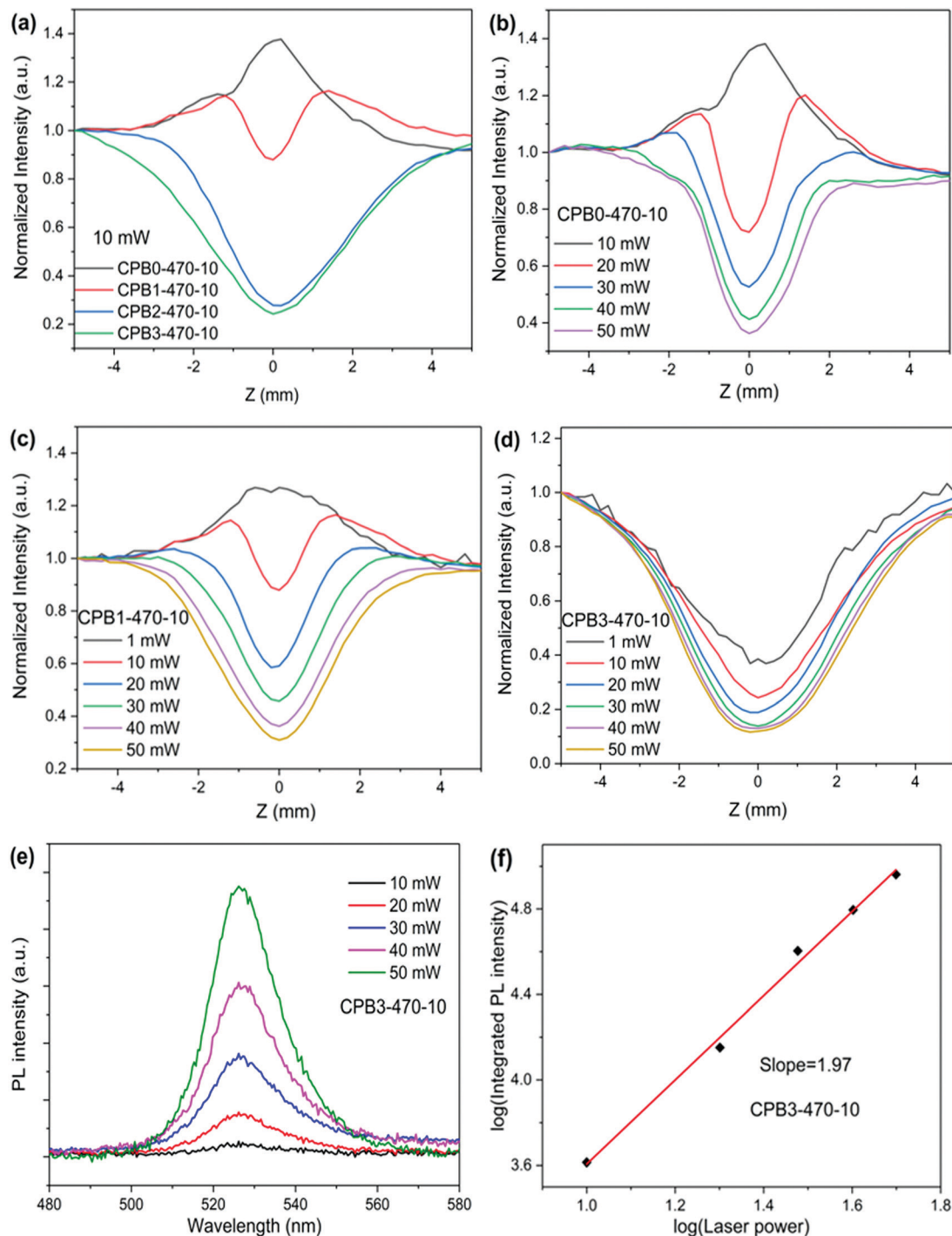
Fig. 5 (a–d) Normalized Z-scan transmittance curves for OA measurement of glass samples. (a) At laser power of 10 mW and (b–d) at different laser powers for the glass samples, (b) CPB0-470-10, (c) CPB1-470-10, and (d) CPB3-470-10. (e) PL spectrum of glass sample CPB3-470-10 recorded under excitation by a 1030 nm fs laser with different laser powers. (f) Laser power-dependent integrated PL intensity of glass sample CPB3-470-10.

Table 3 β and $\mathrm{Im}\chi^{(3)}$ of glass sample CPB3-470-10 at different laser powers

P (mW)	1	10	20	30	40	50
β (10^{-12} m W^{-1})	10.99	1.32	0.71	0.50	0.38	0.31
$\mathrm{Im}\chi^{(3)}$ (10^{-13} esu)	8.29	0.99	0.53	0.37	0.29	0.23

mainly attributed to the absorption by transitions involving excitons and the defect state located within the bandgap.[60,67–71] Due to the effect of quantum confinement, there is an exciton state in the bandgap and its energy is slightly lower than the energy of the direct bandgap,[72–74] as shown in Fig. 6(a). In addition, the presence of defects, e.g., dangling bonds, on the

This journal is © The Royal Society of Chemistry 2021

J. Mater. Chem. C, 2021, **9**, 6863–6872 | **6869**

Fig. 6 Electronic transitions under fs laser excitation. (a and b) Saturable absorption (SA) is induced by single-photon absorption (SPA). (a) Excitonic absorption and (b) defect state absorption. (c) Reverse saturable absorption (RSA) is mainly induced by two-photon absorption (TPA).

QD surfaces may introduce a defect state within the bandgap,[75,76] as shown in Fig. 6(b). Generally, two-photon absorption (TPA) mediated by a virtual state dominates the RSA process for the perovskite QDs,[64,77–79] as shown in Fig. 6(c). Because the energy of the fs laser photon is much lower than the energy of the direct bandgap in our measurement, the defect state absorption plays a dominant role in the SA nonlinear process. According to the XRD results in Fig. 1(c), with the increase of the CaF_2 concentration, the quality of the QDs increases, and the defects on the QD surface are passivated, thereby reducing the defect state absorption, which leads to weakening of the SA process and eventually transitions to the RSA process, as shown in Fig. 5(a). Under the fs laser excitation with low pulse energy, the observed SA process dominates the NLA process for the samples CPB0-470-10 and CPB1-470-10, as shown in Fig. 5(b) and (c). With the increase of laser power, the SA process becomes saturated and the TPA process mediated by a virtual state begins to dominate the NLA process for the samples CPB0-470-10 and CPB1-470-10, resulting in the change from the SA process to the RSA process, as shown in Fig. 5(b) and (c).

In order to explore the RSA mechanism of $CsPbBr_3$ QD-doped glass, the excitation energy-dependent PL spectrum was recorded under excitation by the fs laser ($\sim$1030 nm), as shown in Fig. 5(e) and (f). The PL intensity increases with the increase in the laser pulse energy. A nearly linear relationship between the logarithm of excitation energy and the logarithm of integrated PL intensity is obtained, giving a slope of 1.97 for the sample CPB3-470-10, which indicates that TPA dominates the RSA process in the $CsPbBr_3$ perovskite QD-doped glass.

4. Conclusion

We have demonstrated the tuning of linear and nonlinear optical properties of $CsPbBr_3$ perovskite QD-doped glass by modulating the network topology through the introduction of a network modifier, CaF_2. The precipitation of the QDs and the optical properties of the samples are strongly affected by the introduced metal fluoride network modifier and the PLQY

values could be increased by over 300% under optimal conditions. In addition, the modification of the glass network structure also allows for the control of absorptive optical nonlinearity between saturable absorption and reverse saturable absorption. The strategy demonstrated in the present work can be further exploited for tailoring the optical properties of photonic glasses.

Conflicts of interest

The authors declare no conflict of interest.

Acknowledgements

References

1 Y. T. Dong, Y. K. Wang, F. L. Yuan, A. Johnston, Y. Liu, D. X. Ma, M. J. Choi, B. Chen, M. Chekini, S. W. Baek, L. K. Sagar, J. Fan, Y. Hou, M. J. Wu, S. Lee, B. Sun, S. Hoogland, R. Quintero-Bermudez, H. Ebe, P. Todorovic, F. Dinic, P. C. Li, H. T. Kung, M. I. Saidaminov, E. Kumacheva, E. Spiecker, L. S. Liao, O. Voznyy, Z. H. Lu and E. H. Sargent, *Nat. Nanotechnol.*, 2020, **15**, 668–674.

2 X. Luo, R. Lai, Y. Li, Y. Han, G. Liang, X. Liu, T. Ding, J. Wang and K. Wu, *J. Am. Chem. Soc.*, 2019, **141**, 4186–4190.

3 X. Huang, Q. Guo, D. Yang, X. Xiao, X. Liu, Z. Xia, F. Fan, J. Qiu and G. Dong, *Nat. Photonics*, 2020, **14**, 82–88.

4 K. B. Lin, J. Xing, L. N. Quan, F. P. G. De Arquer, X. W. Gong, J. X. Lu, L. Q. Xie, W. J. Zhao, D. Zhang, C. Z. Yan, W. Q. Li, X. Y. Liu, Y. Lu, J. Kirman, E. H. Sargent, Q. H. Xiong and Z. H. Wei, *Nature*, 2018, **562**, 245–248.

6870 | *J. Mater. Chem. C*, 2021, **9**, 6863–6872

This journal is © The Royal Society of Chemistry 2021

5   Y. Wang, M. I. Dar, L. K. Ono, T. Y. Zhang, M. Kan, Y. W. Li, L. J. Zhang, X. T. Wang, Y. G. Yang, X. Y. Gao, Y. B. Qi, M. Gratzel and Y. X. Zhao, *Science*, 2019, **365**, 591–595.

6   J. S. Yao, J. Ge, B. N. Han, K. H. Wang, H. B. Yao, H. L. Yu, J. H. Li, B. S. Zhu, J. Z. Song, C. Chen, Q. Zhang, H. B. Zeng, Y. Luo and S. H. Yu, *J. Am. Chem. Soc.*, 2018, **140**, 3626–3634.

7   T. Chiba, S. Ishikawa, J. Sato, Y. Takahashi, H. Ebe, S. Ohisa and J. Kido, *Adv. Opt. Mater.*, 2020, **8**, 2000289.

8   R. H. Liu, J. Q. Zhang, H. Zhou, Z. H. Song, Z. N. Song, C. R. Grice, D. J. Wu, L. P. Shen and H. Wang, *Adv. Opt. Mater.*, 2020, **8**, 1901735.

9   Y. H. Lin, N. Sakai, P. Da, J. Y. Wu, H. C. Sansom, A. J. Ramadan, S. Mahesh, J. L. Liu, R. D. J. Oliver, J. Lim, L. Aspitarte, K. Sharma, P. K. Madhu, A. B. Morales-Vilches, P. K. Nayak, S. Bai, F. Gao, C. R. M. Grovenor, M. B. Johnston, J. G. Labram, J. R. Durrant, J. M. Ball, B. Wenger, B. Stannowski and H. J. Snaith, *Science*, 2020, **369**, 96–102.

10 I. Poli, U. Hintermair, M. Regue, S. Kumar, E. V. Sackville, J. Baker, T. M. Watson, S. Eslava and P. J. Cameron, *Nat. Commun.*, 2019, **10**, 2097.

11 C. J. Qin, A. S. D. Sandanayaka, C. Y. Zhao, T. Matsushima, D. Z. Zhang, T. Fujihara and C. Adachi, *Nature*, 2020, **585**, 53–57.

12 P. Y. Cao, B. B. Yang, F. Zheng, L. Wang and J. Zou, *Ceram. Int.*, 2020, **46**, 3882–3888.

13 J. M. Hoffman, J. Strzalka, N. C. Flanders, I. Hadar, S. A. Cuthriell, Q. Zhang, R. D. Schaller, W. R. Dichtel, L. X. Chen and M. G. Kanatzidis, *Adv. Mater.*, 2020, **32**, 2002812.

14 X. Zhang, X. Y. Gao and X. Meng, *J. Alloys Compd.*, 2019, **810**, 151943.

15 Z. Y. Ni, C. X. Bao, Y. Liu, Q. Jiang, W. Q. Wu, S. S. Chen, X. Z. Dai, B. Chen, B. Hartweg, Z. S. Yu, Z. Holman and J. S. Huang, *Science*, 2020, **367**, 1352–1358.

16 V. V. Belykh, D. R. Yakovlev, M. M. Glazov, P. S. Grigoryev, M. Hussain, J. Rautert, D. N. Dirin, M. V. Kovalenko and M. Bayer, *Nat. Commun.*, 2019, **10**, 1746.

17 J. Lapano, M. Brahlek, L. Zhang, J. Roth and R. Engel-Herbert, *Nat. Commun.*, 2019, **10**, 2464.

18 F. M. Li, B. A. Davidson, R. Sutarto, H. Shin, C. Liu, I. Elfimov, K. Foyevtsova, F. Z. He, G. A. Sawatzky and K. Zou, *Phys. Rev. Mater.*, 2019, **3**, 100802.

19 H. T. Zhang, L. R. Dedon, L. W. Martin and R. Engel-Herbert, *Appl. Phys. Lett.*, 2015, **106**, 233102.

20 C. Y. Wang, H. Lin, X. Q. Xiang, Y. Cheng, Q. M. Huang, Y. Gao, X. S. Cui and Y. S. Wang, *J. Mater. Chem. C*, 2018, **6**, 9964–9971.

21 S. N. Chen, *J. Mater. Sci.: Mater. Electron.*, 2019, **30**, 19536–19540.

22 Y. Ye, W. C. Zhang, Z. Y. Zhao, J. Wang, C. Liu, Z. Deng, X. J. Zhao and J. J. Han, *Adv. Opt. Mater.*, 2019, **7**, 1801663.

23 Y. Zhou, C. Liu, Z. Y. Zhao, W. C. Zhang, K. Li, Y. Ye, C. F. Zhu and X. G. Meng, *J. Alloys Compd.*, 2020, **827**, 154349.

24 Z. S. Xu, X. F. Liu, J. R. Qiu and C. Cheng, *Opt. Lett.*, 2019, **44**, 5626–5629.

25 K. Zhang, D. C. Zhou, J. B. Qiu, Z. W. Long, R. Zhu, Q. Wang, J. N. Lai, H. Wu and C. C. Zhu, *J. Am. Ceram. Soc.*, 2020, **103**, 2463–2470.

26 S. S. Li, L. J. Nie, S. M. Ma, G. P. Yao, F. M. Zeng, X. Y. Wang, C. Y. Sun, G. X. Hu and Z. M. Su, *J. Eur. Ceram. Soc.*, 2020, **40**, 3270–3278.

27 Y. Q. Zhang, J. M. Liu, H. L. Zhang, Q. Y. He, X. J. Liang and W. D. Xiang, *J. Eur. Ceram. Soc.*, 2020, **40**, 6023–6030.

28 P. P. Li, Y. M. Duan, Y. Lu, A. Xiao, Z. Y. Zeng, S. Q. Xu and J. J. Zhang, *Nanoscale*, 2020, **12**, 6630–6636.

29 E. Erol, O. Kibrisli, M. C. Ersundu and A. E. Ersundu, *Chem. Eng. J.*, 2020, **401**, 126053.

30 Y. Liu, W. Chen, J. Zhong and D. Chen, *J. Eur. Ceram. Soc.*, 2019, **39**, 4275–4282.

31 D. Chen, S. Yuan, J. Chen, J. Zhong and X. Xu, *J. Mater. Chem. C*, 2018, **6**, 12864–12870.

32 Y. Wang, R. Zhang, Y. Yue, S. Yan, L. Zhang and D. Chen, *J. Alloys Compd.*, 2020, **818**, 152872.

33 P. P. Li, W. Q. Xie, W. Mao, Y. Tian and J. J. Zhang, *J. Alloys Compd.*, 2019, **817**, 153338.

34 X. Z. Zhang, L. Z. Guo, Y. H. Zhang, C. H. Cheng, Y. Cheng, X. P. Li, J. S. Zhang, S. Xu, Y. Z. Cao, J. S. Sun, L. H. Cheng and B. J. Chen, *J. Am. Ceram. Soc.*, 2020, **103**, 5028–5035.

35 D. Chen, Y. Liu, C. Yang, J. Zhong, S. Zhou, J. Chen and H. Huang, *Nanoscale*, 2019, **11**, 17216–17221.

36 G. Lakshminarayana, E. M. Weis, B. L. Bennett, A. Labouriau, D. J. Williams, J. G. Duque, M. Sheik-Bahae and M. P. Hehlen, *Opt. Mater.*, 2012, **35**, 117–125.

37 X. Tian, S. Lian, C. Ji, Z. Huang, J. Wen, Z. Chen, H. Peng, S. Wang, J. Li, J. Hu and Y. Peng, *J. Alloys Compd.*, 2019, **784**, 628–640.

38 R. E. Youngman and M. J. Dejneka, *J. Am. Ceram. Soc.*, 2002, **85**, 1077–1082.

39 K. X. Han, P. Zhang, S. B. Wang, Y. Y. Guo, D. C. Zhou and F. X. Yu, *Sci. Rep.*, 2016, **6**, 31207.

40 A. Maaoui, M. Haouari, A. Bulou, B. Boulard and H. Ben Ouada, *J. Lumin.*, 2018, **196**, 1–10.

41 Y. P. Peng, X. Q. Yuan, L. Zhang, P. G. Yan, W. F. Zhang and S. C. Ruan, *J. Rare Earths*, 2019, **37**, 487–491.

42 Z. S. Xu, X. F. Liu, C. Jiang, D. W. Ma, J. J. Ren, C. Cheng and J. R. Qiu, *J. Am. Ceram. Soc.*, 2018, **101**, 1508–1515.

43 S. L. Kang, X. Q. Song, X. J. Huang, J. R. Qiu and G. P. Dong, *Opt. Mater. Express*, 2016, **6**, 2351–2359.

44 A. H. Mir, I. Monnet, B. Boizot, C. Jégou and S. Peuget, *J. Nucl. Mater.*, 2017, **489**, 91–98.

45 L. G. Jacobsohn, D. F. Franceschini, I. V. Afanasyev-Charkin, D. W. Cooke, L. L. Daemen, R. D. Averitt and M. Nastasi, *Surf. Coat. Technol.*, 2006, **200**, 6079–6082.

46 J. Wu, Y. L. Wang and C. T. Kuo, *Surf. Coat. Technol.*, 2006, **200**, 3303–3308.

47 J. OJensen, *J. Mol. Struct.: THEOCHEM*, 2004, **676**, 193–202.

48 X. W. Miao, Z. T. Bai, X. T. Huo, M. Guo, F. Q. Cheng and M. Zhang, *Ceram. Int.*, 2019, **45**, 8510–8517.

49 Y. Suzuki, T. Park, K. Hachiya and T. Goto, *J. Fluorine Chem.*, 2020, **238**, 109616.

50 Z. G. Zhang, H. Wang and M. Zhu, *Int. J. Hydrogen Energy*, 2011, **36**, 8203–8208.

This journal is © The Royal Society of Chemistry 2021

J. Mater. Chem. C, 2021, **9**, 6863–6872 | **6871**

51 I. S. Peretyazhko, S. Z. Smirnov, A. R. Kotelnikov and Z. A. Kotelnikova, *Russ. Geol. Geophys.*, 2010, **51**, 349–368.

52 T. Wang, Z. Yang, L. L. Yang, X. Yu, L. T. Sun, J. B. Qiu, D. C. Zhou, W. Lu, S. F. Yu, Y. Lin and X. H. Xu, *J. Phys. Chem. Lett.*, 2020, **11**, 4618–4624.

53 K. S. Hun, K. D. Park and S. L. Hong, *Energies*, 2021, **14**, 275.

54 J. B. Zhang, L. W. Fan, J. L. Li, X. F. Liu, R. W. Wang, L. Wang and G. L. Tu, *Nano Res.*, 2019, **12**, 121–127.

55 R. H. Xu, S. Z. Zhao, K. J. Yang, G. Q. Li, T. Li and D. C. Li, *Opt. Express*, 2018, **26**, 8542–8549.

56 X. Zheng, Y. W. Zhang, R. Z. Chen, X. A. Cheng, Z. J. Xu and T. Jiang, *Opt. Express*, 2015, **23**, 15616–15623.

57 M. A. Ali, Y. H. Xian, X. F. Liu and J. R. Qiu, *J. Phys. Chem. C*, 2019, **123**, 9394–9399.

58 G. H. Fan, S. L. Qu, Q. A. Wang, C. J. Zhao, L. Zhang and Z. G. Li, *J. Appl. Phys.*, 2011, **109**, 023102.

59 X. Zheng, R. Z. Chen, G. Shi, J. W. Zhang, Z. J. Xu, X. A. Cheng and T. Jiang, *Opt. Lett.*, 2015, **40**, 3480–3483.

60 Y. T. Ye, Y. H. Xian, J. W. Cai, K. C. Lu, Z. Z. Liu, T. C. Shi, J. Du, Y. X. Leng, R. F. Wei, W. Q. Wang, X. F. Liu, G. Bi and J. R. Qiu, *Adv. Opt. Mater.*, 2019, **7**, 1800579.

61 J. Z. Li, H. X. Dong, B. Xu, S. F. Zhang, Z. P. Cai, J. Wang and L. Zhang, *Photonics Res.*, 2017, **5**, 457–460.

62 Z. S. Xu, Q. B. Guo, C. Liu, Z. J. Ma, X. F. Liu and J. R. Qiu, *Appl. Phys. B: Lasers Opt.*, 2016, **122**, 259.

63 Q. B. Guo, Y. D. Cui, Y. H. Yao, Y. T. Ye, Y. Yang, X. M. Liu, S. Zhang, X. F. Liu, J. R. Qiu and H. Hosono, *Adv. Mater.*, 2017, **29**, 1700754.

64 Z. S. Xu, T. Chen, D. D. Zhang, G. J. Zheng, J. H. Wu, J. H. Yan, X. F. Liu and J. R. Qiu, *J. Eur. Ceram. Soc.*, 2021, **41**, 729–734.

65 W. G. Lu, C. Chen, D. Han, L. Yao, J. Han, H. Zhong and Y. Wang, *Adv. Opt. Mater.*, 2016, **4**, 1732–1739.

66 M. Jin, X. Liang, H. Zhang, J. Liu and Y. Song, *J. Eur. Ceram. Soc.*, 2020, **40**, 4140–4147.

67 D. Mao, S. Zhang, Y. Wang, X. Gan, W. Zhang, T. Mei, Y. Wang, Y. Wang, H. Zeng and J. Zhao, *Opt. Express*, 2015, **23**, 27509–27519.

68 S. Wang, H. Yu, H. Zhang, A. Wang, M. Zhao, Y. Chen, L. Mei and J. Wang, *Adv. Mater.*, 2014, **26**, 3538–3544.

69 G. W. Liang, L. H. Zeng, Y. H. Tsang, L. L. Tao, C. Y. Tang, P. K. Cheng, H. Long, X. Liu, J. Li, J. L. Qu and Q. Wen, *J. Mater. Chem. C*, 2018, **6**, 7501–7511.

70 L. Zhang, S. Fahad, H. R. Wu, T. T. Dong, Z. Z. Chen, Z. Q. Zhang, R. T. Liu, X. P. Zhai, X. Y. Li, X. Fei, Q. W. Song, Z. J. Wang, L. C. Chen, C. L. Sun, Y. Peng, Q. Wang and H. L. Zhang, *Nanoscale Horiz.*, 2020, **5**, 1420–1429.

71 S. L. Jiang, J. Yang, Y. P. Shi, J. Zhao, C. Y. Xie, L. Y. Zhao, J. T. Fu, P. F. Yang, Y. H. Huan, Q. Xie, H. C. Jiang, Q. Zhang, X. L. Wang, F. H. Su and Y. F. Zhang, *Nano Res.*, 2020, **13**, 667–675.

72 Q. J. Han, W. Z. Wu, W. L. Liu, Q. X. Yang and Y. Q. Yang, *Opt. Mater.*, 2018, **75**, 880–886.

73 M. L. De Giorgi, A. Perulli, N. Yantara, P. P. Boix and M. Anni, *J. Phys. Chem. C*, 2017, **121**, 14772–14778.

74 Y. H. Qiu, F. Nan, Q. Wang, X. D. Liu, S. J. Ding, Z. H. Hao, L. Zhou and Q. Q. Wang, *J. Phys. Chem. C*, 2017, **121**, 6916–6923.

75 J. Kang and L. W. Wang, *J. Phys. Chem. Lett.*, 2017, **8**, 489–493.

76 R. Brakkee and R. M. Williams, *Appl. Sci.*, 2020, **10**, 3061.

77 R. Ketavath, N. K. Kattur, S. G. Ghugal, H. K. Kolli, T. Swetha, V. R. Soma and B. Murali, *J. Phys. Chem. Lett.*, 2019, **10**, 5577–5584.

78 K. Wei, Z. J. Xu, R. Z. Chen, X. Zheng, X. G. Cheng and T. Jiang, *Opt. Lett.*, 2016, **41**, 3821–3824.

79 J. Zhang, T. Jiang, X. Zheng, C. Shen and X. A. Cheng, *Opt. Lett.*, 2017, **42**, 3371–3374.

6872 | *J. Mater. Chem. C*, 2021, **9**, 6863–6872

This journal is © The Royal Society of Chemistry 2021